An image processing system for qualitative and quantitative volumetric analysis of brain images

†Alberto F. Goldszal, Ph.D.

§Christos Davatzikos, Ph.D.

*†Dzung L. Pham, M.S.E.

‡Michelle X. H. Yan, Ph.D.

§R. Nick Bryan, M.D., Ph.D.

†Susan M. Resnick, Ph.D.

†*Laboratory of Personality & Cognition, Gerontology Research Center, National Institute on Aging, National Institutes of Health, 5600 Nathan Shock Drive, Baltimore, MD 21224 USA*

§ *Department of Radiology and Radiological Science, The Johns Hopkins University School of Medicine, 600 N. Wolfe St., Baltimore, MD 21287 USA*

* *Department of Electrical and Computer Engineering, The Johns Hopkins University, Baltimore, MD 21218 USA*

‡ *Department of Psychiatry, University of Pennsylvania, Philadelphia, PA 19104 USA*

Blinded Title Page:

An image processing system for qualitative and quantitative volumetric analysis of brain images

Proposed running head:

Analyzing global and regional brain volumes

Correspondence author:

Alberto F. Goldszal, Ph.D.

National Institutes of Health

National Institute on Aging, GRC, LPC

5600 Nathan Shock Drive, Suite 2C20

Baltimore, MD 21224-6825 USA

Tel: (410) 558-8624

Fax: (410) 558-8108

Email: goldszal@nih.gov

ABSTRACT

In this work, we developed, implemented and validated an image processing system for qualitative and quantitative volumetric analysis of brain images. This system allows the visualization and quantitation of global and regional brain volumes. Global volumes were obtained via an automated adaptive Bayesian segmentation technique which labels the brain into white matter, gray matter and cerebrospinal fluid. Absolute volumetric errors for these compartments ranged between 1–3% as indicated by phantom studies. Quantitation of regional brain volumes was performed through normalization and tessellation of segmented brain images into the Talairach space with a 3-D elastic warping model. Retest reliability of regional volumes measured in Talairach space indicated errors of less than 1.5% for the frontal, parietal, temporal and occipital brain regions. Additional regional analysis was performed with an automated, hybrid method combining a region-of-interest approach and voxel-based analysis named Regional Analysis of Volumes Examined in Normalized Space (RAVENS). RAVENS analysis for several subcortical structures showed good agreement with operator-defined volumes. This system has sufficient accuracy for longitudinal imaging data and is currently being used in the analysis of neuroimaging data of the Baltimore Longitudinal Study of Aging (BLSA).

INTRODUCTION

The precise quantification of structural changes that occur in the brain with aging or disease has been an area of active research in neuroimaging for many years. To accurately characterize brain structure and any anatomic changes which may occur over time, and to correlate such anatomical changes with concurrent physiological or cognitive changes, we developed, implemented, and validated a set of imaging tools capable of capturing subtle longitudinal changes in the regional and global volumetric structure of the brain. We tested this system on cross-sectional and longitudinal magnetic resonance (MR) imaging data acquired as part of the neuroimaging study of participants in the Baltimore Longitudinal Study of Aging (BLSA) (1). The main goal of this image processing system is to measure the magnitude, rate and regional pattern of longitudinal changes in the brain. Future applications are extensible to functional neuroimaging data. All system components have known accuracy and errors, and thus, the overall system accuracy can be estimated.

The application of an image processing system within a large scale longitudinal brain imaging study has posed difficulties in the development, implementation and validation of the different components. Methods typically employed in cross-sectional studies do not have sufficient sensitivity to detect more subtle longitudinal changes. Most studies focusing on the volumetric analysis of the brain deal with cross-sectional data and seek the measurement of part of or the total volume of a structure or region of interest (2–6). Although the notion that imaging studies employing quantitative volumetric methods potentially yield more accurate and less biased results than qualitative studies is widely accepted, validating this assumption can be difficult and time-consuming. Quantitative neuroanatomic methods may range from manual, local operations in 2-D images (7) to automated, 3-D model-based brain volume estimations (2, 8) to continuous, automated, 3-D volumetric measurements based on probabilistic atlases of neuroanatomy (9–12). Detailed cortical parcellation techniques have been developed (13), but they are extremely laborious and time-consuming. In addition, these approaches usually depend on subjective criteria, leading to

difficulties in establishing reliability and validity. Finally, an extensive literature exists on stereological methods (14, 15), which, however, are suitable only for volumetric measurements of large partitions; detecting small local changes by fine sampling would require a prohibitive amount of work.

In our case, we are interested in accurately, reliably and automatically measuring the total volumes of structures and regions in the brain. We are particularly concerned with the ability to capture small structural brain changes which may occur over time at global and regional (local) levels. The quantitative methods used in our system include the acquisition of 3-D high-resolution MR spoiled grass (SPGR) images, pre-processing of the data, image segmentation, normalization and regional volumetric analyses including the volumetric quantification of MR images within a stereotaxic coordinate system.

At the center of this image processing system are the segmentation and normalization techniques. Our segmentation approach (16) has the ability to adapt to shading artifacts caused by non-uniformities in the radiofrequency (RF) field during image acquisition. Shading artifacts, which occur in nearly all MR images, cause voxel intensities of the same tissue class to vary over the image domain. These artifacts may be corrected prior to the image segmentation step (17–20) or their correction may be embedded within the segmentation procedure (16, 21–23). In the former case, an algorithm first compensates for the shading artifact, then the image is segmented by one of the several available segmentation techniques (24). In the latter group, the intensity inhomogeneities are compensated simultaneously with image segmentation. In either case, not compensating for the shading artifacts might severely limit the accuracy of any segmentation technique operating on MR images. In addition to shading artifacts, our approach is also very robust to poor soft tissue contrast, low signal-to-noise ratio and partial volume effects.

The segmentation allows quantitative measures of global changes in the brain, however, additional tools are necessary to measure the local magnitude and regional pattern of longitudinal changes in the brain. To quantify regional volumes, we examine the brain images within a standard stereotaxic space, the Talairach coordinate space (25), after spatially normalizing all images for

overall shape differences. Several methodologies for spatial normalization of brain images have been proposed in the literature (25–34). Our approach is based on a geometric deformable model, coded in the STAR algorithm, which uses a surface-based elastic warping transformation to bring two 3-D images into registration (35, 36). This technique has superior performance and better accuracy than other normalization methods which are based on a piecewise linear Talairach transformation (2) or normalization approaches employed by statistical parametric mapping (SPM) (32) because it utilizes several explicit features, e.g., the ventricular boundary, as well as the outer cortical surface, to drive the elastic transformations. The use of the ventricular boundaries and cortical features is particularly critical in the presence of atrophy, a situation common in the elderly.

For the regional analysis in stereotaxic space, the segmented data are tessellated into the 1,056 Talairach boxes (25). This method yields an accurate and reliable approach for quantitation of large brain regions; however, due to the discrete nature of the Talairach boxes, it is not suitable for smaller regions or individual brain structures. For the quantitation of smaller brain regions, we employ a hybrid procedure which combines the stability of a region-of-interest (ROI) approach with the spatial resolution of a voxel-based method. We refer to this alternate procedure as Regional Analysis of Volumes Examined in Normalized Space, or RAVENS.

MATERIALS AND METHODS

System Overview. Image analysis is comprised of several steps including reslicing of the data, removal of extracranial tissues, segmentation of different tissue types, normalization to a standard coordinate space, and regional quantitative analysis. A schematic diagram illustrating the overall procedure is shown in Figure 1. In this section, we describe each component in greater detail.

MRI Acquisition. While the main goal of this paper is to present an image analysis methodology, we tested our protocols on a small sample of elderly subjects — a subset of the participants in the Baltimore Longitudinal Study of Aging (1). All subjects in this study were

scanned with a GE Signa 1.5 T scanner (GE Medical Systems, Waukesha, WI) employing a T1-weighted Spoiled GRASS (SPGR) pulse sequence. The parameters of the SPGR sequence were TR = 35 ms, TE = 5 ms, flip angle = 45°, image size = 256 x 256 x 124 voxels, and voxel size = 0.9375 x 0.9375 x 1.5 mm^3.

Image Reformatting. After acquisition, the images were resliced parallel to the AC-PC plane using (i) the correctional angles for roll, yaw, and pitch determined interactively, and (ii) cubic splines for interpolation of the data running on a Silicon Graphics $Indigo^2$ high-impact workstation (Silicon Graphics Inc., Mountain View, CA).

Removal of Extracranial Tissues. An important pre-processing step is the removal of extracranial tissues because our segmentation technique labels the entire brain into three global compartments: WM, GM and CSF. Removal of extracranial tissues is also important for the stereotaxic normalization which is based on the brain boundaries as opposed to the skull contour.

Removal of extracranial tissues was accomplished by a sequential application of morphological operators, thresholding, seeding, region growing, and manual editing. First, a morphological erosion with a spherical structuring element (default radius = 2 mm) detaches the brain tissue from the surrounding dura. Next, a 3-D seeded region growing extracts the brain tissue. Finally, a 3-D morphological dilation with a spherical structuring element (default radius = 4 mm) recaptures the tissue lost in the erosion step. Note that the radius of the sphere used in the dilation is larger than the one used in the erosion in order to guarantee that no brain tissue is lost either due to the manual thresholding or to the erosion. In addition, whenever users assign a narrow threshold range, holes may be created inside the brain region. As long as these holes are not connected to the image background, they are automatically recognized as brain regions and filled with the original voxel values. If needed, bridges are placed to sever any connection of these holes with the background.

This automated step takes less than a minute (running on a SGI Indigo^2) to generate a "deskulled" image set. A limitation of this method for pre-processing SPGR images is that an undetermined amount of sulcal CSF is removed because the CSF-dura interface is difficult to determine reliably with the SPGR pulse sequence. Thus, sulcal CSF cannot be estimated reliably from our SPGR images. Typically, the automated step generates an image which is adequate for many image processing operations, such as registration and 3-D rendering. However, for a quantitative volumetric analysis of brain images, some manual editing was necessary to extract the sagittal sinus anteriorly and posteriorly, to eliminate extracranial tissues mesial to the temporal lobes, and to remove portions of the dura posteriorly. In addition, prior to the segmentation step, we manually edited out the cerebellum and brainstem due to concerns about the adequacy of our segmentation algorithm to accurately label these regions and our emphasis on quantitative analysis of the cerebrum. Figures 2A–C illustrate, for a single brain slice, the complete removal process of extracranial tissues.

Quantitation of Global Brain Volumes. Following the removal of extracranial material, each voxel in the brain-extracted image is labeled into WM, GM and CSF using a 3-D generalization of the method developed by Yan *et al.* (16). This technique segments single- or multi-spectral brain images into *m*-different tissue types where, in our study, $m = 3$ for WM, GM and CSF. Each scalar-valued image (e.g., a MR SPGR volume) is modeled as a collection of regions with slowly varying intensity, described by B-spline functions, plus white Gaussian noise. Spatial smoothness of the segmentation is obtained by modeling voxel dependencies by a 3-D, second order Markov Random Field (MRF).

The algorithm maximizes the *a posteriori* probability jointly over tissue types and mean intensities in an iterative and adaptive fashion. For each iteration, it estimates (i) the mean intensities for each tissue type via a least squares fitting of the B-spline function, and (ii) the tissue type regions modeled by a MRF. By increasing the number of control points of the B-spline

functions, the algorithm slowly adapts to regional intensity variations which, in the case of MR images, may be caused by shading artifacts due to MR field inhomogeneities.

The segmentation algorithm is fully automated. As an initial step, the algorithm pre-segments the data with a *k*-means clustering technique which groups the voxels in the image into *k* clusters through the minimization of the total inter-cluster variance (a maximum likelihood estimation). The result of the pre-segmentation is then used as an initial classification for the adaptive and iterative model. After the automated segmentation into WM, GM and total CSF, the ventricular CSF (V-CSF) was determined by manually drawing a crude ROI to eliminate any CSF falling outside the ventricular system. This ROI served as a mask within which CSF voxels on the segmented image were reclassified as V-CSF.

Image Normalization. The segmented images provide global volumetric measurements of the total amount of WM, GM and V-CSF. To quantify regional brain volumes, however, the images were examined within a standard stereotaxic space, the Talairach reference space (25), after spatially normalizing all images for global morphological differences. The spatial normalization of the images was performed using the STAR algorithm detailed in (35, 36).

Briefly, a parametric representation of the outer boundary of the brain was first determined from the skull-stripped images, using the deformable surface algorithm developed by Davatzikos (36). Based on this representation, a map from the outer boundary of each subject's brain to the brain of the Talairach atlas (25) was obtained. This map was determined by maximizing the similarity of geometric characteristics between the subject's brain and the brain of the atlas. For example, the outer edges of the inter-hemispheric and Sylvian fissures, which have high curvature, are recognized and matched by the algorithm.

Subsequently, each image was elastically warped to satisfy the outer cortical map, accounting for the overall shape differences in the subjects' brains. Additionally, variability in ventricular size was accounted for using a uniform strain within the ventricles. This procedure allowed their contraction corresponding to volumetric differences between each subject's ventricles

and the ventricles in the atlas. After this gross volumetric correction, a force field applied to the ventricular boundaries brought them into register with the ventricular boundaries in the atlas. Ventricular registration is an important step in our normalization procedure because we are imaging older subjects who, typically, have enlarged ventricles compared with younger subjects. The rest of the brain tissue was deformed according to the equations governing the deformation of an elastic solid.

Another important characteristic of our spatial normalization procedure is the preservation of the tissue volumetric units in stereotaxic space, rather than the tissue density as is customary in many spatial normalization methods (2, 32). Therefore, the total volumes of WM, GM and V-CSF are the same before and after normalization. It is important to preserve the tissue volumetric units to permit quantitative analyses in stereotaxic space. For example, a volumetric difference between the two hemispheres would otherwise be eliminated after normalization to the symmetric Talairach atlas.

Quantitation of Regional Brain Volumes. The regional quantitative analysis is performed by two distinct methods: the "Boxel" counting method and the RAVENS method. Both approaches quantify brain regions in stereotaxic space and are based on the previously segmented and normalized images. The major differences between the regional quantitation methods are related to resolution and visualization issues. The Boxel method is adequate for quantitation of large compartments like the frontal, temporal, parietal and occipital brain regions (2). The method is fully automated and visualization is not required. The RAVENS approach takes full advantage of visual information and mapping techniques and is best suited for quantitation and visualization of smaller brain regions like the caudate nucleus, the lenticular nucleus, the temporal horns, and potentially, specific cortical ROIs. These regions are not individually labeled by the global segmentation method nor quantified by the Boxel approach. Additionally, the RAVENS method is more flexible and takes advantage of the image's full resolution through a voxel-based analysis. The method can operate in an automated or interactive mode.

The Boxel Method — Tissue Distributions in Talairach Space and Box Analysis. Following normalization, the segmented images were tessellated into 1,056 boxes, as described in (25). The total amounts of WM, GM and V-CSF were measured for each box. These 1,056 measurements could in principle be compared individually across subjects; however, such comparisons would be meaningful only if the normalized images were in perfect register. In practice, this is not the case, due to residual inter-individual variability after normalization. Therefore, measurements at the box level are likely to have higher variance across individuals, which would reduce the statistical significance of morphological changes or differences observed. In addition, each box may include several anatomic regions, limiting the utility of data based on individual boxes.

The individual boxes were thus grouped into larger brain compartments, as defined and validated by Andreasen and colleagues (2). Specifically, we defined four major compartments corresponding to the frontal, temporal, parietal and occipital lobes. Then, after tessellating a segmented brain image into the Talairach space, regional quantitation is obtained by counting the volumes for each tissue type, i.e., WM, GM and V-CSF, within each of the four lobes for each hemisphere.

RAVENS — Regional Analysis of Volumes Examined in Normalized Space. The Boxel method provides a low resolution "boxelated" description of tissue distributions in Talairach space. The RAVENS technique yields a more accurate and flexible analysis that combines the stability and flexibility of an ROI approach with the spatial resolution of a voxel-based method.

The normalization of the images into the Talairach space causes a deformation of the original image morphology; however, applying the RAVENS method, the tissue volumes are preserved by coding them as intensity-based maps. As shown in Figure 3A–D, brain regions which expanded during the normalization step will look darker than their original counterparts because the same amount of tissue was spread over a larger area. Similarly, regions which were decreased in size will look proportionally brighter. Note that after normalization, the shape and size

of both ventricles are similar (as expected) and the differences in volumes are coded as intensity-based maps.

Once the segmented tissue distributions are stereotaxically normalized, they may be averaged to generate mean images for groups or processed individually for longitudinal analyses. Typically, as illustrated in Figure 4A–C, we generate average images over samples of interest and display them as intensity-based maps. Besides being able to carry out quantitative analyses in normalized space, these displays allow for scale-space analysis (by allowing different degrees of blurring) and provide a representation which can be directly correlated with other imaging modalities such as normalized PET scans.

The quantitative analysis of brain structures and regions with the RAVENS maps may be performed in two different ways: (i) a free-hand ROI may be drawn directly on a RAVENS map as illustrated in Figure 5A; integration of the RAVENS map within this ROI yields the volume of the underlying structure. Or, (ii) as illustrated in Figure 5B, a brain structure may be chosen in a co-registered digital brain atlas; this atlas' structure is then overlaid onto the RAVENS map, marking a 3-D region which is integrated through all slices yielding the volume of the structure being studied. This method is particularly attractive to us since many brain regions have already been delineated and defined in a digital stereotaxic atlas of neuroanatomy (37), allowing automated processing of many regions. The volumetric accuracy of this method becomes mainly a function of the global and local registration precision between the digital atlas and the RAVENS maps.

ASSESSMENT OF RELIABILITY AND VALIDITY

Removal of Extracranial Tissues. Since the complete removal of extracranial tissues involved manual editing by an operator, interoperator differences were examined to assess how distinct operators would affect the stripping process. For this test, fourteen images were initially processed with the automated part of the skull stripping method and then manually edited, independently by two operators, for any extracranial tissues still present in the images. Finally,

these two sets of images were segmented and the volumes of the white matter and gray matter compartments compared by t-test.

Image Segmentation — Phantom. To assess the accuracy of the adaptive Bayesian method and to compare it against other segmentation techniques, we created the 3-D digital brain phantom depicted in Figure 6. The overall shape of the phantom and the volume of its three major compartments — WM, GM and CSF — are based on a segmented SPGR image of a 72 year old subject. In this case, the segmentation involved a simple thresholding technique which was complemented by manual outlining. The matrix size of the phantom is 256 x 256 x 72 voxels with each voxel measuring 0.9375 mm^2 x 1.5 mm and having 8-bits of depth. This image set serves as our standard reference, with known volumes for WM, GM and CSF.

A number of parameters may be modified in the phantom to create a realistic looking image (Figure 6A) which simulates the appearance and characteristics of an older brain. These parameters include: mean intensity values, noise, magnetic field inhomogeneities and partial volume effects. The specific parameters employed in our validation studies were determined from MRI scans of ten older individuals aged 59–84 years. Based on these images, mean intensity values of the phantom were fixed at 112.08, 87.53, and 35.00 for the WM, GM and CSF, respectively. The standard deviation of the superimposed Gaussian noise was set to 6.0. The 3-D linear shading which simulated magnetic field inhomogeneities was 7% in each direction. Finally, the partial volume averaging effect of the MR acquisition was simulated substituting each point in the final image by a weighted average in its 6-connected 3-D neighborhood.

Results for the adaptive Bayesian method (Figure 6B) were compared with: a Gaussian clustering method, a *n*-nearest neighbors classifier, and a neural networks technique all implemented in the Analyze biomedical image analysis package (38); a region growing method and a multiple thresholding technique implemented in the MEDx radiological image processing software (Sensor Systems Inc., Sterling, VA); and a standard fuzzy *c*-means algorithm (24).

Short-Term Reliability. To assess the short-term reliability of our quantitative approach, three subjects had repeated SPGR scans separated by approximately 30 minutes with the subjects being removed from the scanner and repositioned between the two SPGR acquisitions. The images were volumetrically acquired, pre-processed to remove extracranial tissues, and segmented into WM, GM and V-CSF.

Longitudinal Stability. To assess the longitudinal or long-term stability of our approach, we examined data from ten BLSA subjects, who had been imaged at times *t* and *t*+1 year. The ten subjects ranged in age from 59–84 years (mean, 72.4 years ± 10.7). SPGR images were acquired approximately one year apart. These images were pre-processed and segmented into WM, GM and V-CSF. However, unlike the short-term reliability study previously described, for a single subject, any observed differences in the volumes of WM, GM and V-CSF compartments between times *t* and *t*+1 year, do not necessarily reflect inconsistencies or errors in the image analysis protocol employed. During a period of one year, it is conceivable that true anatomical changes may take place, altering the volumes of the WM, GM and/or V-CSF. The possibility of true longitudinal brain changes may be particularly relevant for older subjects. Thus, any differences between volumetric measurements at times *t* and *t*+1 year confound measurement errors and true longitudinal changes, and reflect upper-bound estimates of the measurement error.

Regional Brain Volumes — Boxel Analysis. Reliability of the Boxel analysis was assessed using the images from the three subjects with repeated SPGR scans separated by 30 minutes. Following segmentation into WM, GM and V-CSF, the images were tessellated into the Talairach space and regional tissue distributions computed for the frontal, parietal, temporal and occipital regions. Comparisons of the regional tissue distributions between times *t* and *t*+30 minutes provide measures of repeatability.

RAVENS. To illustrate and validate the application of the RAVENS approach for visualization and quantitation of regional brain volumes, average maps were created for the sample of ten subjects aged 59–84 years. The RAVENS method was applied to these maps and three brain regions were quantified: the caudate nucleus, the lenticular nucleus, and the temporal horns. Validation of this approach was accomplished via manual outlining (independently by two operators) and volume computation for the three structures using the original MR images. These volumes were then compared to those obtained with the RAVENS method.

RESULTS

Removal of Extracranial Tissues. The interoperator reliability test revealed that there were only small differences in the manual editing between the two trained operators. For the fourteen image sets evaluated, the average within subject difference between raters was -0.02% ± 1.37 for WM and 0.46% ± 0.88 for GM. Correlations were greater than 0.99 for both measures. Finally, paired t-test comparisons yielded no significant differences between raters.

Quantitation of Global Brain Volumes — Phantom. The results for the comparison of different segmentation methods are presented in Table 1. The adaptive Bayesian technique yielded absolute volumetric errors on the order of 1–3% for each individual compartment and 0.43% for the total brain tissue volume. In addition, the adaptive Bayesian method presented better overall accuracy for segmentation of the WM, GM and CSF volumes of simulated MR SPGR images when compared against all tested approaches. Finally, we also tested the accuracy of our segmentation approach on a different phantom developed by A. C. Evans and colleagues (39) at the Montreal Neurological Institute (http://www.bic.mni.mcgill.ca), obtaining very similar results.

It is also observed that the fuzzy *c*-means algorithm, a very popular algorithm used in brain image segmentation, presented a slightly better result in the segmentation of the CSF compartment, but less accurate measurement of WM and GM volumes. We believe that the adaptive Bayesian

technique presented better overall segmentation results mainly due to its ability to adapt to local image intensity variations caused by shading artifacts due to MR field inhomogeneities.

Short-Term Reliability. The short-term reliability assessment for the three subjects showed that the average absolute volumetric differences between measures at times *t* and *t*+30 minutes for WM, GM, total brain tissue volume, and V-CSF, calculated as |((Scan2 – Scan1)/Scan1)|*100%, were 0.75% ± 0.38, 0.71% ± 0.62, 0.31% ± 0.37, and 0.87% ± 0.93, respectively.

Longitudinal Stability. Longitudinal changes in volumes were calculated as ((Year2 – Year1)/Year1)*100% for the ten subjects studied at times *t* and *t*+1 year. The average longitudinal volumetric differences for WM, GM, total brain volume, and V-CSF were -0.46% ± 2.34, -0.03% ± 1.08, -0.26% ± 1.09, and 3.52% ± 2.21, respectively. Correlations between measurements at time *t* and time *t*+1 year for WM, GM, total brain volume, and V-CSF were, respectively, 0.98, 0.99, 1.00, and 1.00.

Quantitation of Regional Brain Volumes — Boxel Analysis. The results for the Boxel approach are summarized in Table 2 and indicate good repeatability of the overall method. We also used these data to compare the WM, GM, total brain, and V-CSF volumes yielded by the Boxel method and our global segmentation technique. The results showed no volumetric differences between the global segmentation results and Boxel method for the above mentioned compartments. Therefore, as predicted from our design, the normalization and tessellation procedures preserve the tissue volumetric units in stereotaxic space.

RAVENS. The mean volumes and standard deviations found using the manual tracing approach and the RAVENS plus atlas method are presented for the temporal horns, caudate nucleus and lenticular nucleus in Table 3. For all three structures, paired t-tests indicated no significant differences between operator-determined volumes and those calculated using RAVENS. For the

caudate nucleus, the correlations between operator A and operator B, operator A and RAVENS method, and operator B and RAVENS method were, respectively, 0.90, 0.84 and 0.84. For the lenticular nucleus, these correlations were 0.92, 0.85 and 0.79, respectively. Finally, for the temporal horns, the correlations were 0.99, 0.95 and 0.97, respectively. Intraclass correlations among the three estimates were 0.86, 0.86, and 0.95 for the caudate, the lenticular nucleus, and the temporal horns, respectively. Note that it was necessary for the two operators to train on several series of image data sets to achieve acceptable interoperator agreement.

DISCUSSION

In this paper, we presented and validated an image processing system for qualitative and quantitative volumetric analysis of MR images of the brain. The development of the different system components was motivated by our need for an accurate and reliable system capable of analyzing cross-sectional and longitudinal data. The application of this image processing system within the framework of a large scale longitudinal study posed unique difficulties in the development, implementation and validation of the different system components. A general goal of our system is to reliably and accurately analyze and quantify large amounts of volumetric data over a period of years. Specifically, based on the analysis of structural MR data, we want to measure the magnitude, rate and regional pattern of longitudinal changes in the brain. We achieved these goals by designing a system with the following basic characteristics: the accuracy and errors of the individual system components are measurable and known, providing an estimate of the overall system accuracy; the system must be efficiently implemented since large amounts of data are being processed; whenever possible, methods are automated without compromising their accuracy; manual handling of the data is kept at a minimum, and the variability introduced by different operators, when necessary, is measured. Additionally, the MR data are processed in a manner which permits correlation and combination with external measures (e.g., neuropsychological assessments of memory and cognition) and/or other imaging modalities such as PET and other

functional neuroimaging measures. Furthermore, the methods were adapted and optimized to manipulate data sets from older subjects who typically have enlarged ventricular systems and greater degree of brain atrophy.

Our imaging system was divided into five major components or steps: acquisition of the MR data, image pre-processing, global segmentation, stereotaxic normalization and regional volumetric analyses which, in turn, were composed of the Talairach boxes counting method (the 'Boxel' method) and a newly proposed RAVENS method.

Our assessment of the error introduced by trained operators during the image pre-processing step indicated that interoperator variability is less than 1% of WM, GM and total brain volumes. Errors in the tissue labeling ranged between 1–3% for WM, GM and CSF as shown by phantom studies. This accuracy indicates that we have sufficient sensitivity to detect longitudinal volumetric changes greater than 2 to 3% for individual measures of WM, GM and CSF. Furthermore, this technique has the ability to detect longitudinal volumetric changes on the order of 0.5% for the total brain tissue volume. The adaptive Bayesian segmentation technique does better than other segmentation schemes to which it was compared. This is in part due to this technique's refined modeling of the problem and its improved ability to adapt to shading artifacts caused by local inhomogeneities in the magnetic field gradients of the MR scanner. The accuracy of the adaptive Bayesian approach for segmentation of SPGR images is a significant advance, as poor results with prior methods have led to reluctance in using these high resolution images for quantification of WM and GM volumes. This segmentation technique also demonstrated good longitudinal stability. However, establishing actual long-term retest reliability is difficult because true changes in brain structure may occur. Our experiments provide a lower-bound estimate of longitudinal reliability since volumetric measurements over a period of one year confound methodological errors and true anatomical changes.

During normalization, the registration of the ventricular boundaries was an important consideration when processing brain images of older subjects who, typically, have enlarged ventricles and sulci compared with younger subjects. The normalization of the segmented data,

preserving the true volumetric units of the tissue distributions, allowed quantitation within Talairach space. The Boxel approach showed excellent repeatability and short-term stability. Regional absolute volumetric differences between scan-rescan were, in general, less than 1% for all four brain regions. Although our implementation represents a significant improvement over existing methods, it still has limitations associated with the existence of multiple anatomical regions within the individual boxes.

An alternative way to measure regional tissue distributions is the RAVENS approach which allows us to quantify and visualize segmented brain images in normalized space. Particularly, we are able to analyze brain structures which are not quantifiable by the global segmentation method or the Talairach boxes counting approach due to limitations in the accuracy and resolution of these techniques. When used in conjunction with a co-registered digital atlas of neuroanatomy, the RAVENS method is as reliable and accurate as a trained operator for the detection and volume computation of certain brain structures. In addition, the RAVENS approach has the advantage of computing ROI volumes faster and automatically, substantially increasing speed of image processing. Typically, this approach can be used to provide fast processing and efficient screening of large amounts of neuroimaging data. For instance, one can compute the volumes of several different structures and focus further analysis on those structures which revealed greater changes, i.e., those "highlighted" brain structures can be later analyzed with more elaborate and time-consuming techniques.

Although the RAVENS method is capable of handling smaller structures and has better anatomical specificity, it needs validation in the quantification of smaller brain structures like the hippocampus and specific cortical ROIs. Future methodological improvements also include refinements in the registration of the RAVENS maps and the digital atlas of neuroanatomy. With a larger number of natural landmarks being automatically recognized and matched during the normalization, residual registration errors tend to decrease, therefore, improving the quantification accuracy of selected brain structures. Finally, extension of these methods to other imaging acquisition protocols and imaging modalities is also being pursued.

ACKNOWLEDGMENTS

This work was supported in part by NIH contract NIH-AG-93-07. Christos Davatzikos, Ph.D., was supported in part by a Whitaker Foundation research grant. The authors would like to express their gratitude to Cindy B. Quinn, R.N., for helping with several manual image processing tasks and Michael Unser, Ph.D., for providing the spline interpolation algorithm.

REFERENCES

1. Shock NW, Greulich RC, Andres R, et al. *Normal human aging: the Baltimore Longitudinal Study of Aging*. U.S. Public Health Service publication no. NIH 84-2450. Washington, D.C.: U.S. Government Printing Office, 1984.

2. Andreasen NC, Rajarethinam R, Cizadlo T, et al. Automatic atlas-based volume estimation of human brain regions from MR images. *J Comput Assist Tomogr* 1996;20(1):98–106.

3. Jack JCR, Twomey CK, Zinsmeister A, et al. Anterior temporal lobes and hippocampal formations: normative volumetric measurements from MR images in young adults. *Radiology* 1989;172:549–54.

4. Kertesz A, Polk M, Black SE, Howell J. Sex, handedness, and the morphometry of cerebral assymmetries on magnetic resonance imaging. *Brain Res* 1990;530:40–8.

5. Shenton ME, Kikinis R, Jolesz FA, et al. Abnormalities of the left temporal lobe and thought disorder in schizophrenia: a quantitative magnetic resonance imaging study. *N Engl J Med* 1992;327:604–12.

6. Andreasen NC, Ehrhardt JC, Swayze VW, et al. Magnetic resonance of the brain in schizophrenia: the pathophysiological significance of structural abnormalities. *Arch Gen Psychiatry* 1990;47:35–44.

7. Reiss AL, Faruque F, Naidu S, et al. Neuroanatomy of Rett syndrome: a volumetric imaging study. *Ann Neurol* 1993;34:227–234.

8. Collins DL, Holmes CJ, Peters TM, Evans AC. Automatic 3-D model-based neuroanatomical segmentation. *Hum Brain Map* 1995;3:190–208.

9. Evans AC, Kamber M, Collins DL, MacDonald D. An MRI-based probabilistic atlas of neuroanatomy. In: Shorvon SD, et al. Ed. *Magnetic resonance scanning and epilepsy*. New York: Plenum Press, 1994:263–274.

10. Thompson PM, MacDonald D, Mega MS, Holmes CJ, Evans AC, Toga AW. Detection and mapping of abnormal brain structure with a probabilistic atlas of cortical surfaces. *J Comput Assist Tomogr* 1997;21(4):567–581.

11. Haller JW, Christensen GE, Joshi SC, Newcomer JW, Miller MI, Csernansky JG, Vannier MW. Hippocampal MR imaging morphometry by means of general pattern matching. *Radiology* 1996;199:787–791.

12. Davatzikos C, Vaillant M, Resnick S, Prince JL, Letovsky S, Bryan RN. A computerized approach for morphological analysis of the corpus callosum. *J Comput Assist Tomogr* 1996;20:88-97.

13. Rademacher J, Galaburda AM, Kennedy DN, Filipek PA, Caviness VS Jr. Human cerebral cortex: localization, parcellation, and morphometry with magnetic resonance imaging. *J Cogn Neurosci* 1992;4(4):352–374.

14. Roberts N, Cruz-Orive LM, Reid NMK, Brodie DA, Edwards RHT. Unbiased estimation of human body composition by the Cavalieri method using magnetic resonance imaging. *J Microscopy* 1993;171:239–253.

15. Pakkenberg B, Boesen J, Albeck M, Gjerris F. Unbiased and efficient estimation of total ventricular volume of the brain obtained from CT scans by a stereological method. *Neuroradiology* 1989;31:413–417.

16. Yan MXH, Karp JN. An adaptive Bayesian approach to three-dimensional MR brain segmentation. In *Proceedings of XIVth International Conference on Information Processing in Medical Imaging* 1995; pp 201–213.

17. Dawant BM, Zijidenbos AP, Margolin RA. Correction of intensity variations in MR images for computer-aided tissue classification. *IEEE Trans Med Imag* 1993;12:770–781.

18. Meyer CR, Peyton HB, Pipe J. Retrospective correction of intensity inhomogeneities in MRI. *IEEE Trans Med Imag* 1995;14:36–41.

19. Johnston B, Atkins MS, Mackiewish B, Anderson M. Segmentation of multiple sclerosis lesions in intensity corrected multispectral MRI. *IEEE Trans Med Imag* 1996;15:154–169.

20. Lim KO, Pfefferbaum A. Segmentation of MR brain images into cerebrospinal fluid spaces, white and gray matter. *J Comput Assist Tomogr* 1989;13(4):588–593.

21. Pappas TN. An adaptive clustering algorithm for image segmentation. *IEEE Trans on Signal Processing* 1992;40:901–914.

22. Wells WM III, Grimson WEL, Kikinis R, Jolesz FA. Adaptive segmentation of MRI data. *IEEE Trans Med Imag* 1996;15:429–442.

23. Rajapaske JC, Giedd JN, Rapoport JL. Statistical approach to segmentation of single-channel cerebral MR images. *IEEE Trans Med Imag* 1997;16:176–186.

24. Bezdek JC, Hall LO, Clarke LP. Review of MR image segmentation techniques using pattern recognition. *Med Phys* 1993;20:1033–48.

25. Talairach J, Tournoux P. Co-planar stereotaxic atlas of the human brain. New York: Thieme Medical, 1988.

26. Bookstein FL. Principal warps: thin-plate splines and the decomposition of deformations. *IEEE Trans Patt Anal Mach Intell* 1989;11:567–85.

27. Bajcsy R, Kovacic S. Multiresolution elastic matching. *Comput Vis Graph Image Proc* 1989;46:1–21.

28. Gee JC, Reivich M, Bajcsy R. Elastically deforming 3D atlas to match anatomical brain images. *J Comput Assist Tomogr* 1993;17:225–36.

29. Miller MI, Christensen GE, Amit Y, Grenander U. Mathematical textbook of deformable neuroanatomies. *Proc Natl Acad Sci USA* 1993;90:11944–8.

30. Collins DL, Neelin P, Peters TM, Evans AC. Automatic 3D intersubject registration of MR volumetric data in standardized Talairach space. *J Comput Assist Tomogr* 1994;18:192–205.

31. Friston KJ, Holmes AP, Worseley KJ, Poline J-B, Frith CD, Frackowiak RSJ. Statistical parametric maps in functional imaging: a general linear approach. *Hum Brain Map* 1995;2:189–210.

32. Friston KJ, Ashburner J, Frith CD, Poline J-B, Heather JD, Frackowiak RSJ. Spatial registration and normalization of images. *Hum Brain Map* 1995;2:165–189.

33. Lancaster JL, Glass TG, Bhujanga RL, Downs H, Mayberg H, Fox PT. A modality-independent approach to spatial normalization of tomographic images of the human brain. *Hum Brain Map* 1995;3:209–223.

34. Martin RF, Bowden DM. A stereotaxic template atlas of the macaque brain for digital imaging and quantitative neuroanatomy. *Neuroimage* 1996;4:119–150.

35. Davatzikos C. Spatial normalization of 3D brain images using deformable models. *J Comput Assist Tomogr* 1996;20(4):656–665.

36. Davatzikos C, Bryan RN. Using a deformable surface model to obtain a shape representation of the cortex. *IEEE Trans Med Imag* 1996;15(6):785–795.

37. Nowinski WL, Bryan RN, Raghavan R. *The electronic clinical brain atlas on CD-ROM*. New York: Thieme Medical, 1997.

38. Robb RA. A software system for interactive and quantitative analysis of biomedical images. In: Höhne KH, Fuchs H, Pizer SM, eds. *3D imaging in medicine*. NATO ASI Series, Vol. F60, pp. 333–361, 1990.

39. Cocosco CA, Kollokian V, Kwan RK-S, Evans AC. BrainWeb: online interface to a 3-D MRI simulated brain database. *Neuroimage* 1997;5(4):S425.

TABLE 1

Segmentation Errors

Technique	Absolute Volumetric Error† (in %)		
	WM	**GM**	**CSF**
Adaptive Bayesian	2.71	-1.96	1.67
Gaussian Clustering	-5.15	-21.36	15.49
***n*-Nearest Neighbors**	4.86	-8.22	8.89
Neural Networks	5.15	-8.69	6.22
Region Growing	-27.46	-9.73	-16.80
Thresholding	32.73	-9.89	-10.77
Fuzzy *C*-Means	19.61	-9.88	0.95

† $Absolute\ Volumetric\ Error = \frac{estimated\ compartment\ vol - true\ compartment\ vol}{true\ compartment\ vol} x\ 100\%$

TABLE 2

Repeatability of the Boxel method in Talairach space. Numbers represent the average volumetric differences (in percentage)[§] between measurements based on MR scans at times *t* and *t*+30 minutes for three subjects. Standard deviations are also shown

Brain Region	Tissue Type		
	WM	**GM**	**Total Brain Matter**
Frontal	-0.34% ± 2.34	-1.09% ± 1.73	–0.72% ± 1.94
Parietal	-0.80% ± 1.68	-1.20% ± 2.24	-0.99% ± 1.96
Temporal	0.99% ± 1.52	0.67% ± 1.00	0.81% ± 1.19
Occipital	0.79% ± 1.50	0.52% ± 1.64	0.65% ± 1.30

§ $\frac{Scan2 - Scan1}{Scan1} * 100\%$

TABLE 3

Volumetric measurements (in mm^3) of the caudate nucleus, the lenticular nucleus and the temporal horns obtained manually by trained operators and automatically by a combination of the RAVENS maps and a digital brain atlas. Data reflect measurements on ten subjects

Brain Region	Method		
	Operator A	Operator B	RAVENS + atlas
Caudate Nucleus	5777.3 ± 917.3	5787.7 ± 726.4	5788.8 ± 937.1
Lenticular nucleus	6815.3 ± 551.7	6807.2 ± 580.0	6818.0 ± 468.6
Temporal Horns	1568.1 ± 1242.7	1349.1 ± 1000.7	1399.3 ± 1051.5

FIGURE CAPTIONS

FIGURE 1

Schematic diagram of our image analysis system.

FIGURE 2

Illustration of the different steps involved in the removal of extracranial tissues for a single MR slice. In 2A, a brain slice oriented parallel to the AC-PC plane; in 2B, subsequent to processing by the automated "deskulling" algorithm; and in 2C, after the additional manual editing step. Note that the major differences between 2B and 2C are the dura and sagittal sinus posteriorly (marked by arrow heads).

FIGURE 3

With the RAVENS method, the tissue volumetric units are coded in Talairach space as intensity-based representations, allowing quantitative measurements to be performed in normalized space. For instance, two male subjects both aged 74 years, whose brains are depicted in 3A and 3C, have ventricular volumes of 57,227 mm^3 and 27,749 mm^3, respectively. The normalized representations of the ventricles illustrated in 3A and 3C are shown in 3B and 3D, respectively. Note that the larger ventricle, 3A, yields a brighter map in normalized space as indicated by 3B. Conversely, the smaller the ventricle, 3C, has a dimmer representation in normalized space as indicated by 3D. The image intensity values in 3B and 3D are proportional to the original ventricular volumes in 3A and 3C, respectively.

FIGURE 4

Illustration of the RAVENS maps for a sample population of ten subjects aged 59–84 years (mean, 72.4 years ± 10.7). In 4A–C, respectively, the average WM, average GM and average V-CSF for the ten subjects are represented in stereotaxic space (single slices through the 3-D volumes are

depicted). Brighter areas correspond to regions with relatively more tissue volume whereas darker areas show regions containing less tissue volume. Black areas depict total absence of tissue class.

FIGURE 5

Applications of the RAVENS method. In 5A, manual outline of the lenticular nucleus is done directly on a RAVENS map representing the average GM tissue for a sample population. Integration of these hand drawn outlines over the entire 3-D image yields the volume of the underlying brain structure. In 5B, the same procedure is done automatically. The lenticular nucleus, in red, is chosen in a co-registered digital brain atlas, a 3-D mask is created and overlaid onto the RAVENS map, and the volume of the structure being studied is computed after integrating for all slices.

FIGURE 6

Digital brain phantom. In 6A, our digital phantom after specification of the parameters used to create a realistic looking MR image which simulates the appearance and characteristics of an older brain; in 6B, segmentation of the image shown in 6A with the adaptive Bayesian technique into WM, GM and CSF compartments.

FIGURE 1

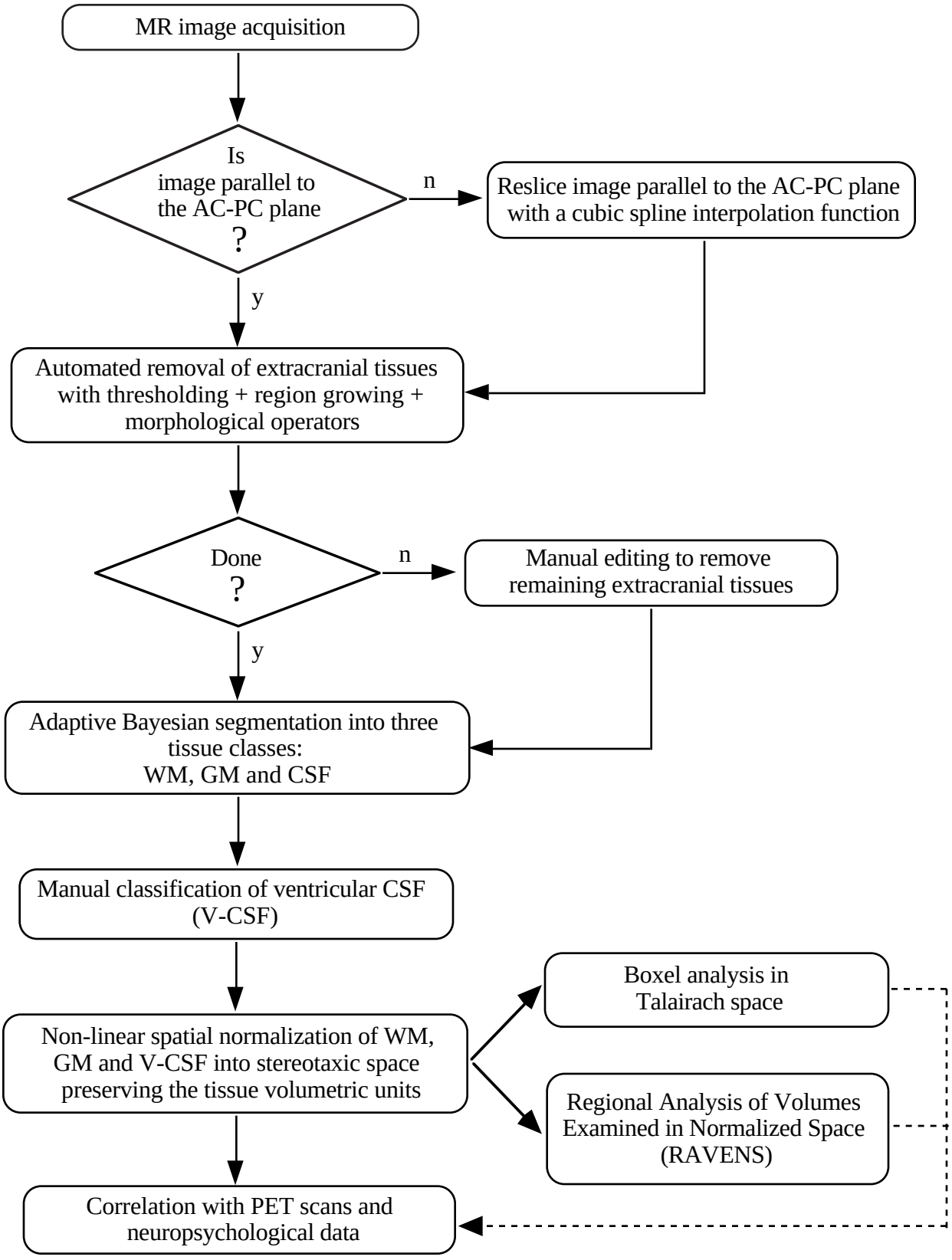
MR image acquisition
Is image parallel to the AC-PC plane ?
n
Reslice image parallel to the AC-PC plane with a cubic spline interpolation function
y
Automated removal of extracranial tissues with thresholding + region growing + morphological operators
Done ?
n
Manual editing to remove remaining extracranial tissues
y
Adaptive Bayesian segmentation into three tissue classes: WM, GM and CSF
Manual classification of ventricular CSF (V-CSF)
Non-linear spatial normalization of WM, GM and V-CSF into stereotaxic space preserving the tissue volumetric units
Boxel analysis in Talairach space
Regional Analysis of Volumes Examined in Normalized Space (RAVENS)
Correlation with PET scans and neuropsychological data

FIGURE 2

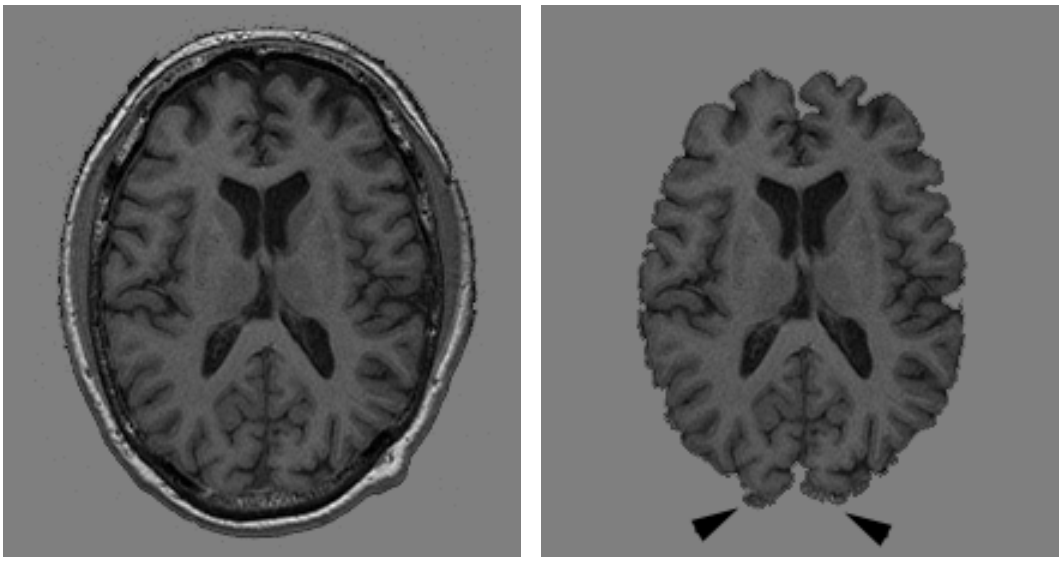

(A) **(B)**

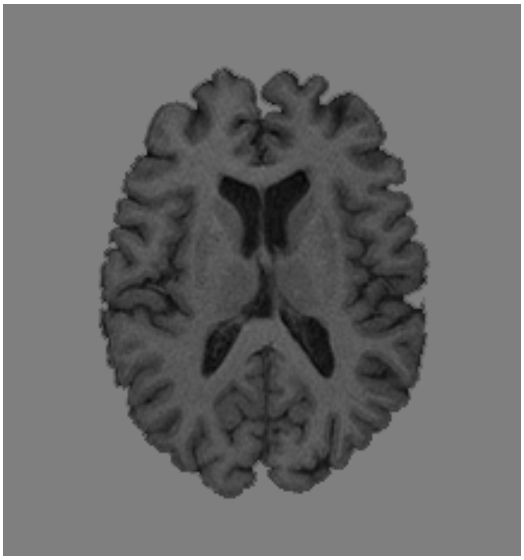

(C)

FIGURE 3

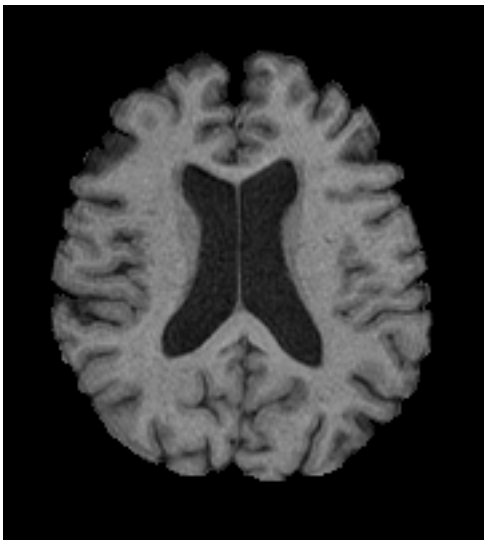

(A)

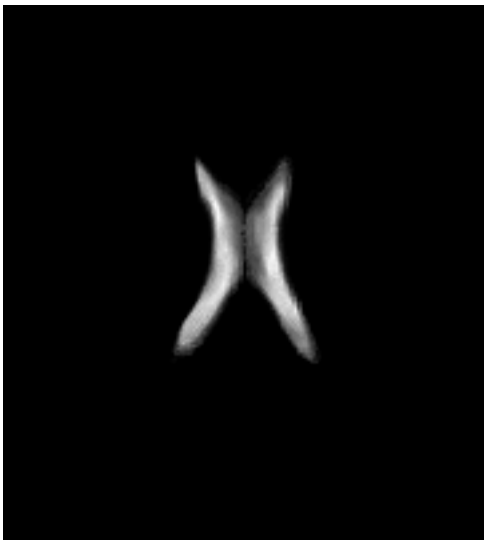

(B)

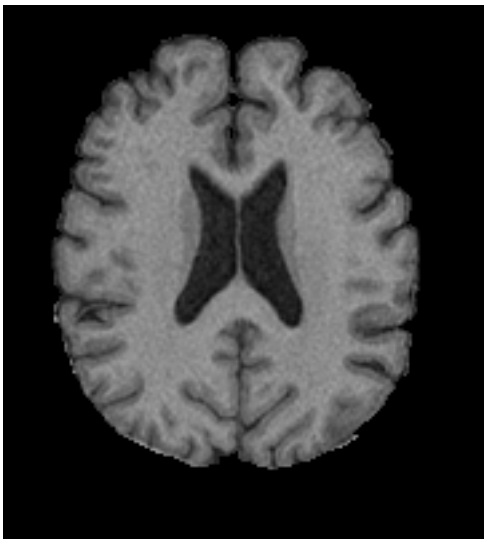

(C)

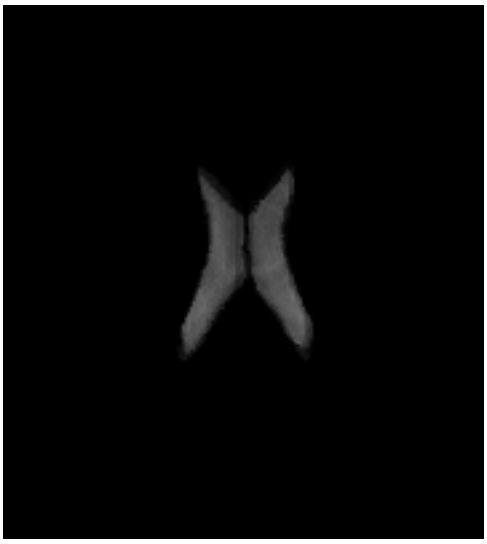

(D)

FIGURE 4

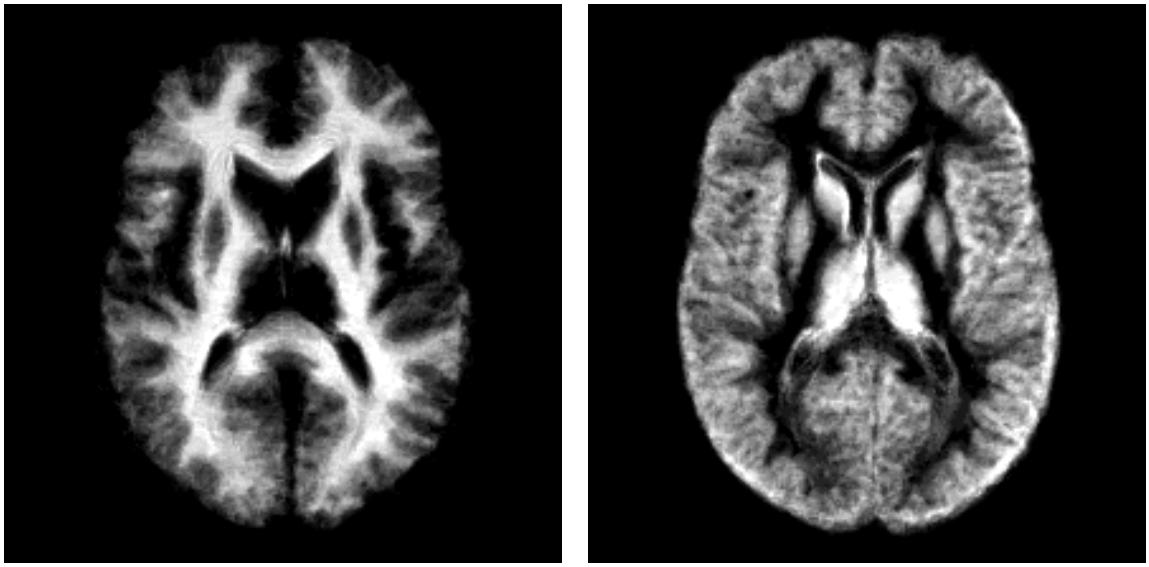

(A) **(B)**

(C)

FIGURE 5

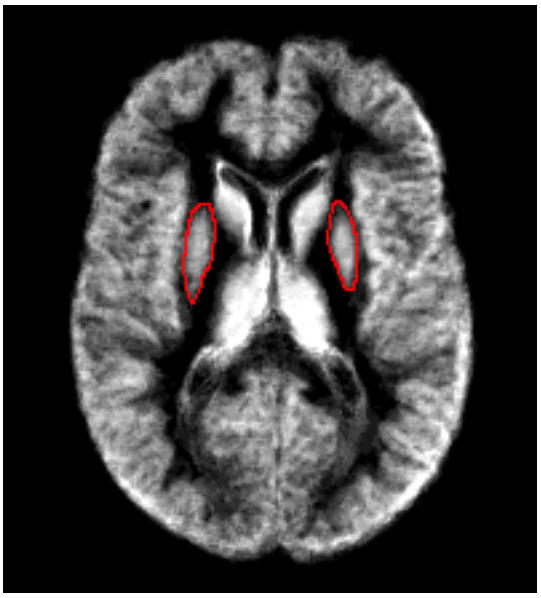

(A)

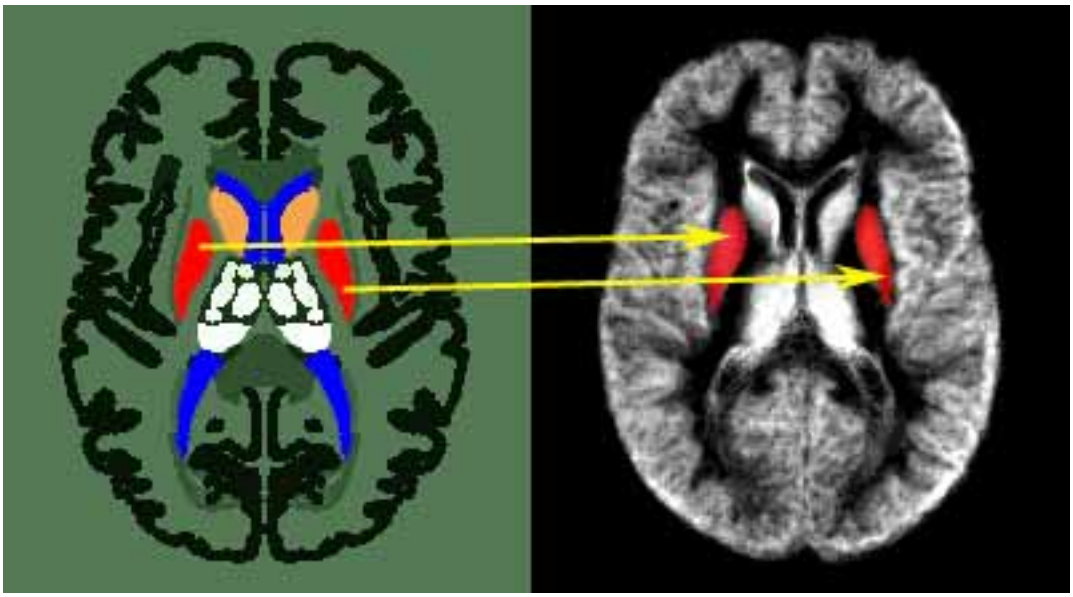

(B)

FIGURE 6

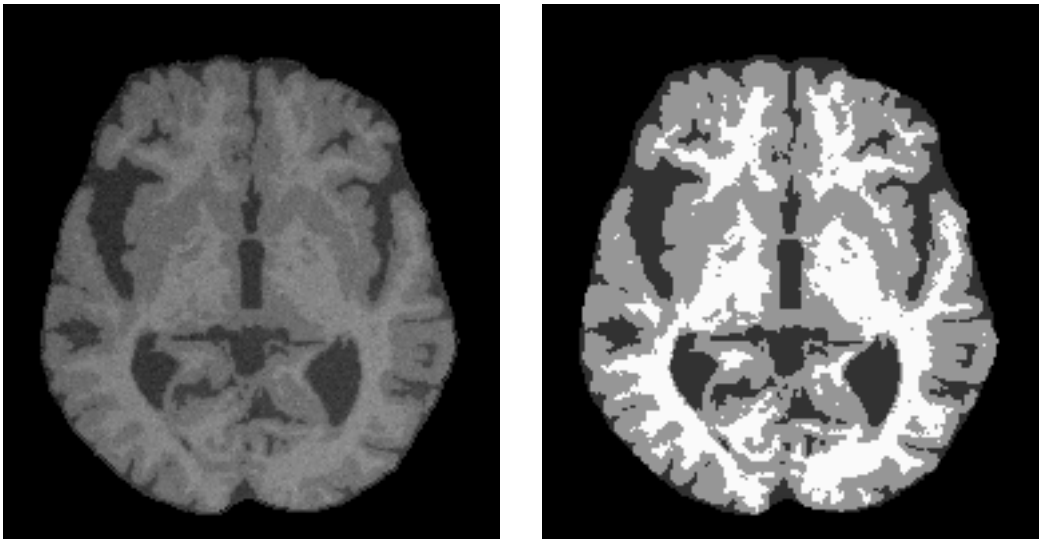

(A) **(B)**